


Cite this: *Mater. Adv.*, 2023,
4, 4835

Synthesis of a new photosensitizer for photodynamic and photothermal synergistic cancer therapy†

Jun Deng,^{*a} Xiaohua Xia,^a Hua Yuan,^a Zhiqiang Chen,^b Xin Jiang,^b
Dengfeng Zou ^{*b} and Qiang Wang^{*a}

Semiconducting compounds have tremendous potential for phototherapeutic treatment of cancer, owing to their high reactive oxygen species (ROS) generation ability and photothermal conversion efficiency. In this paper, we report a newly synthesized photosensitizer, PDIDPP for the treatment of human colon (HCT-116) and Uppsala 87 malignant glioma (U87MG) cancer cells. Nanoparticles (NPs) with uniform size were synthesized by encapsulating DSPE-PEG₂₀₀₀ (1,2-distearoyl-*sn*-glycero-3-phosphoethanolamine-*N*-[methoxy(polyethylene glycol)-2000]) onto the surface of PDIDPP. Such NPs show outstanding ROS generation ability and photothermal conversion efficiency (32.6%) with light irradiation. *In vitro* investigation indicates that these NPs can be uptaken by U87MG and HeLa cells and considerable phototoxicity was observed with irradiation, while the dark toxicity was negligible. Further *in vivo* study showed that tumor proliferation was completely inhibited with the help of a laser, while the normal organs suffered from no adverse effects. These results suggest that PDIDPP NPs may be potential candidates for cancer phototheranostics.

Received 12th July 2023,
Accepted 8th September 2023

DOI: 10.1039/d3ma00400g

rsc.li/materials-advances

Introduction

Cancer has become the leading cause of death, and people in growing numbers are dying of cancer every year.¹ Traditional therapies, such as chemotherapy and radiotherapy, usually lack targeting ability and sometimes have severe side effects on normal tissues.^{2–4} Phototherapy, referring to photodynamic (PDT) and photothermal therapy (PTT), has advantages over chemotherapy, for instance, non-invasiveness, no-drug resistance and less side effects.^{5–8} Photosensitizers (PSs) play a vital role in phototherapy because they can undergo intersystem crossing (ISC) to sensitize the surrounding oxygen for the generation of cytotoxic reactive oxygen species (ROS) for photodynamic therapy (PDT).^{9–15} Besides, non-radioactive transition usually leads to the generation of heat for photothermal therapy (PTT). It would, therefore, be an efficient approach to enhancing the therapeutic efficacy when combining PDT and PTT, in terms of synergistic therapy. Ideal PSs should possess low dark toxicity as well as high phototoxicity to maximize the phototherapy efficacy and simultaneously minimize the side

effects.^{16–21} PDT and PTT synergistic therapy may compensate for each other, thus enhancing the therapeutic efficacy. Rational design of an anticancer strategy contributes to precise cancer therapy. Designing nanomaterials with advanced functions and physical properties to improve cancer diagnosis and treatment has been a tremendous challenge.

Semiconducting compounds have been universally used for biomedical applications, including imaging and therapy, due to their excellent thermal stability, high ROS generation and photothermal conversion efficiency.^{22–25} They are usually combined with drug delivery, afterglow imaging and photodynamic therapy.^{26–33} For example, Chen *et al.* reported an *in situ* polymerization in perylene diimide hybridized hollow mesoporous organosilica nanoparticles for phototheranostics.³⁴ Among the various semiconducting compounds, heavy atom free compounds can minimize the potential dark toxicity of the photosensitizers and reduce the systemic toxicity.^{9,23}

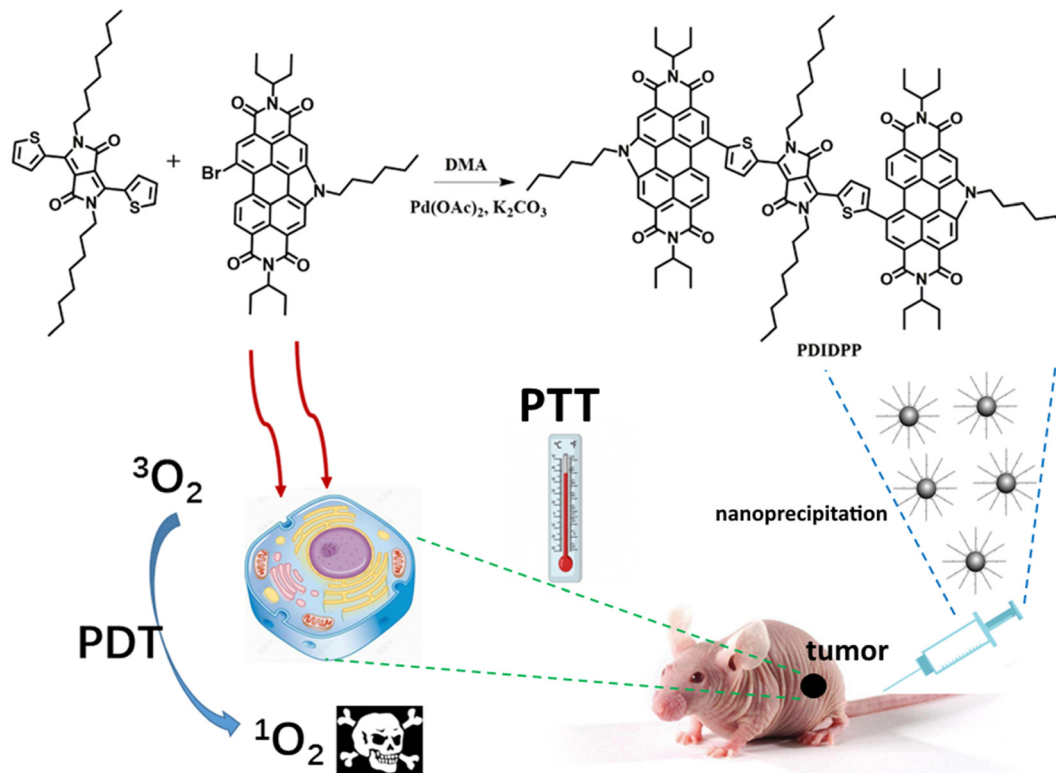
In this paper, we are devoted to designing and synthesizing a new semiconducting compound for phototherapy against cancer cells. PDIDPP ((11,11'-(5,5'-(2,5-dioctyl-3,6-dioxo-2,3,5,6-tetrahydropyrrolo[3,4-c]pyrrole-1,4-diyl)bis(thiophene-5,2-diyl))bis(5-hexyl-2,8-di(pentan-3-yl)-1H-pyrido[3',4',5':4,5]naphtha [2,1,8-cde]-pyrido[3',4',5':4,5]naphtho[8,1,2-ghi]isoindole-1,3,7,9(2H,5H,8H)-tetraone)) was prepared by a C–H activation reaction (Scheme 1). Nanoprecipitation was used to prepare water dispersible NPs with a spherical morphology and the average diameter is 62 nm. Such NPs can be efficiently uptaken by U87MG and HCT-116

^a Department of Emergency Surgery, Kunshan Hospital Affiliated to Jiangsu University Kunshan, 215300, Jiangsu, P.R. China. E-mail: yaya850830@126.com, wq.516@163.com

^b School of Pharmacy, Guilin Medical University, Guilin, 541004, Guangxi, P.R. China. E-mail: zdf1226@126.com

† Electronic supplementary information (ESI) available. See DOI: <https://doi.org/10.1039/d3ma00400g>





Scheme 1 Synthetic route of PDIDPP NPs for phototheranostics.

cells. The outstanding ROS generation ability and photothermal conversion efficiency (23.6%) of the PDIDPP NPs promise excellent phototoxicity. Further flow cytometry results also indicate that PDIDPP NPs can induce cell apoptosis with laser irradiation. Further *in vivo* study showed that the tumor proliferation was completely inhibited with the help of a laser while the normal organs suffered from no adverse effect. The results show that PDIDPP NPs can be potential candidates for cancer treatment.

Experimental section

Synthesis and characterization of PDIDPP

A mixture of DPP (200.0 mg, 0.24 mmol), 11-bromo-5-hexyl-2,8-di(pentan-3-yl)-1*H*-pyrido[3',4',5':4,5]naphtho[2,1,8-cde]pyrido[3',4',5':4,5]naphtho[8,1,2-ghi]isoindole-1,3,7,9 (2*H*, 5*H*,8*H*)-tetraone (423 mg, 0.60 mmol), Pd(OAc)₂ (22.0 mg, 0.04 mmol) and K₂CO₃ (83.0 mg, 0.60 mmol) was dissolved in 5 mL DMA. Then N₂ was bubbled to drive off possible oxygen and water in the system. The mixture was heated to 110 °C under the protection of N₂ gas for 12 h. After cooling to room temperature, the mixture was poured into saturated brine (150 mL) and extracted with dichloromethane (100 mL) three times. The organic layer was washed with brine, followed by drying with anhydrous sodium sulfate. The solvent was removed by rotary evaporation, and then purified by silica gel column chromatography with dichloromethane and hexane (1:2, v/v) as the developing solvent. Dark blue solids were obtained (Yield: 95 mg, 30%). ¹H NMR: δ 9.40–9.35(2*H*, d),

9.15–9.05 (2*H*, d), 8.89 (2*H*, s), 8.66–8.58 (2*H*, d), 8.37–8.31 (2*H*, d), 7.76–7.60 (2*H*, d), 5.29–5.15 (5*H*, m), 5.00–4.92 (4*H*, t), 2.45–2.20 (13*H*, m), 2.01–1.93 (9*H*, m), 1.93–1.82 (5*H*, m), 1.54–1.45 (6*H*, m), 1.45–1.35 (7*H*, m), 1.36–1.24 (9*H*, m), 1.23–1.14 (5*H*, m), 1.14–1.08 (8*H*, m), 1.04–0.92 (23*H*, m), 0.92–0.85 (7*H*, m), 0.74–0.66 (6*H*, m). ¹³C NMR: 161.47, 147.76, 139.64, 132.74, 132.47, 131.87, 128.76, 127.92, 124.73, 123.00, 119.60, 108.41, 57.94, 47.01, 42.45, 31.28, 30.07, 28.92, 26.91, 25.21, 22.36, 13.73, 11.18. MS: *m/z*: 1774.84, found: 1775.11.

Singlet oxygen detection and photothermal conversion efficiency

Singlet oxygen generation was detected using 1,3-diphenylisobenzofuran (DPBF) as the ¹O₂ indicator. Generally, a mixture of DPBF and PDIDPP was prepared and the absorbance of DPBF was adjusted to 1.0 while that of PDIDPP is 0.2 to 0.3. After irradiation for different periods of time, the absorbance spectra were recorded.

PDIDPP NPs were irradiated by light (660 nm, 0.5 W cm⁻²) and then cooled to room temperature. The temperature was recorded by a near-infrared camera. The photothermal conversion efficiency was calculated according to eqn (1)–(5).

$$\eta = \frac{h\nu(T_{\max} - T_{\text{amb}}) - Q_{\text{Dis}}}{I(1 - 10^{-A_{660}})} \quad (1)$$

$$\theta = \frac{T - T_{\text{amb}}}{T_{\text{Max}} - T_{\text{amb}}} \quad (2)$$



$$dt = -\tau_s \frac{d\theta}{\theta} \quad (3)$$

$$\tau_s = \frac{\sum_i m_i C_{p,i}}{hs} \quad (4)$$

$$t = -\tau_s \ln(\theta) \quad (5)$$

where h , S and T_{\max} stand for the heat transfer coefficient, surface area of the container, and highest temperature of PDIDPP NPs in water at the maximum steady-state temperature, respectively. I , Q_{Dis} and A_{660} represent the laser power density (0.5 W cm^{-2}), the heat associated with light absorption by the solvent and the absorbance of the PDIDPP NPs at 660 nm, respectively. The variable τ_s , m_i and C_i are the sample-system time constant, the mass, and the heat capacity of the deionized water ($4.2 \times 10^3 \text{ J kg}^{-1} \text{ }^\circ\text{C}^{-1}$), respectively.

Cell culture, cellular uptake and fluorescence imaging of cellular ROS

Human glioblastoma cells (U87MG) and human colorectal carcinoma (HCT-116) were cultured with medium consisting of 12% fetal bovine serum (FBS) in DMEM (Gibco) under the atmosphere of 5% CO_2 . U87MG and HCT-116 cells were cultured with PDIDPP NPs (3 mL) in a confocal dish for 4 h. Then the medium was discarded and the cells were washed with PBS three times (1 mL), followed by co-culture with 1 mL polyoxymethylene for 25 min. Then polyoxymethylene was discarded and the cells were also washed with PBS three times (1 mL). The cells were further co-cultivated with DCF-DA (2,7-dichlorodihydrofluorescein diacetate, 10 μmol) for 5 min, followed by washing with PBS (1 mL) three times. The samples were irradiated by an LED lamp for 3 minutes (0.5 W cm^{-2}). The cells were excited at 633 nm and the fluorescence was collected from 600 to 750 nm (red channel). For the *in vitro* ROS detection, the cells were excited at 488 nm and the fluorescence was collected from 490 to 560 nm.

Cytotoxicity towards U87MG and HCT-116 cells

PDIDPP NPs with different concentrations were co-cultured with U87MG or HCT-116 cells in a 96-well plate. For the irradiation group with or without NPs, each well was irradiated with an LED for 10 minutes. Relative cell viability was determined by the MTT assay by recording the absorbance of MTT (3-(4,5-dimethylthiazol-2-yl)-2,5-diphenyltetrazolium bromide). MTT in PBS (5 mg mL^{-1}) was added to the well (20 μL) and then incubated for 4 h. After that, the medium was discarded and DMSO (200 μL) was added. The absorbance of each well was recorded on a Bio-Tek microplate reader. Cell viability was then calculated according to the equation:

Cytotoxicity (%)

$$= \frac{\text{mean absorbance of the group incubated with PDIDPP NPs}}{\text{mean absorbance of the control group}}$$

In vivo study

In this study, all animal experiments were performed following the guidelines of Guilin Medical University and approved by the Institutional Animal Care and Use Committee (IACUC) of Guilin Medical University. The U87MG cell line was chosen as the tumor model. 200 μL DPPPDI NP ($200 \mu\text{g mL}^{-1}$) solution in saline was intravenously administered into nude mice. When the tumor volume reached around 100 mm^3 , the nude mice were randomly assigned to three groups ($n = 5$) with different treatments: (i) saline + laser (control), (ii) PDIDPP NPs only, and (iii) PDIDPP NPs with irradiation. The tumors of the control and illumination groups were irradiated by a laser (660 nm, 0.5 W cm^{-2}). Tumor volume (V) was measured every two days according to the following equation:

$$V = \frac{\text{length} \times \text{width}^2}{2}$$

Statistical analysis

All quantitative data in this study were presented as mean \pm standard deviation from at least 3 independent experiments. The significance between the two groups was analyzed by a two-tailed Student's *t*-test. For multiple comparisons, one-way analysis of variance (ANOVA) with Tukey's *post hoc* test was used. Statistical analysis was performed using GraphPad Prism 6.0. *P* values of less than 0.05 were considered significant ($*P < 0.05$, $**P < 0.01$, $***P < 0.001$).

Results and discussion

Synthesis and generation characterization of PDIDPP and NPs

PDIDPP was synthesized by a C–H activation reaction (Scheme) and characterized by ^1H NMR, ^{13}C NMR and mass spectroscopy, the results of which suggest the high purity of the compound (Fig. S1–S3, ESI †). Then nanoprecipitation was used to prepare water dispersible nanoparticles (NPs) by encapsulating DSPE-PEG-2000 onto the surface of PDIDPP. Transmission electron microscopy (TEM) and dynamic light scattering (DLS) indicate that PDIDPP NPs can assemble into spherical morphology with an average diameter of 62 nm (Fig. 1a and b). The main absorbance peak lies at 530 nm in THF while that in water at 591 nm. Therefore, a red shift (61 nm) could be observed for the absorbance of PDIDPP NPs, compared with that in tetrahydrofuran (THF). Meanwhile, a long Stokes shift (60 nm) was also observed in the fluorescence emission in THF and an even longer one (83 nm) for that in water (Fig. 1c and d). This phenomenon is attributed to both the solvent effect and the aggregation of PDIDPP NPs in aqueous solution.

Singlet oxygen generation and photothermal conversion efficacy

High singlet oxygen generation ability promises excellent phototherapeutic efficacy. Therefore, the $^1\text{O}_2$ QY of PDIDPP was calculated by recording the absorbance of 1,3-diphenylisobenzofuran (DPBF) with laser irradiation. As shown in Fig. 2a and b, the absorbance of DPBF continues to decrease with laser irradiation, indicating the ROS generation.



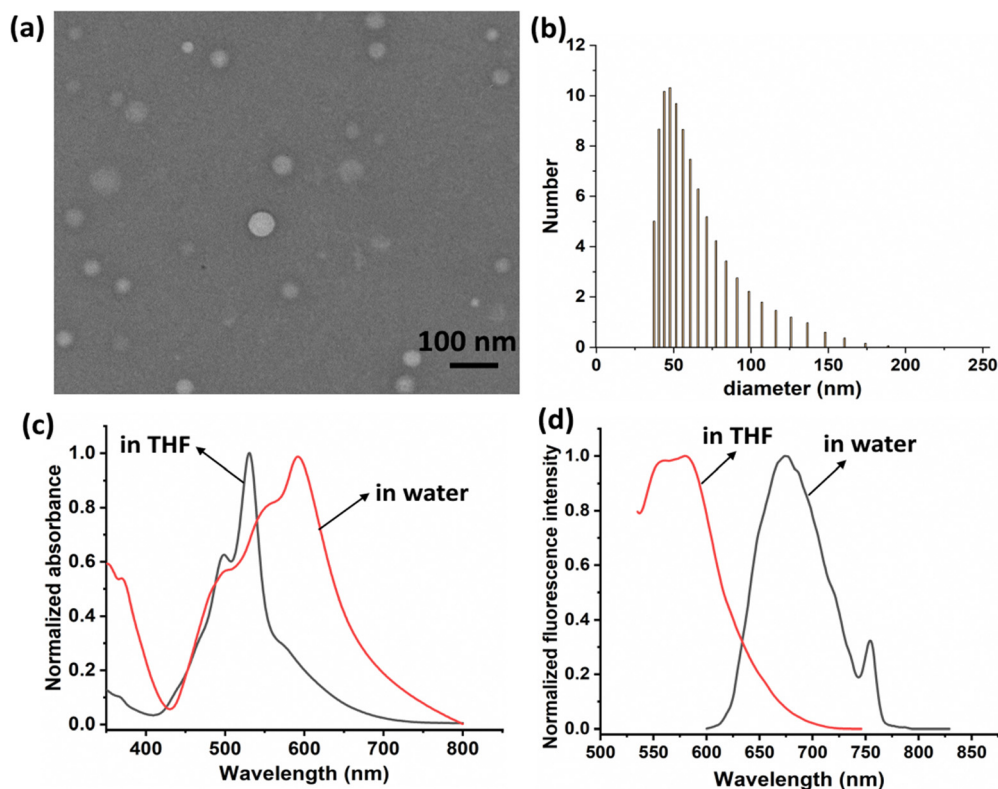


Fig. 1 (a) Transmission electron microscopy of PDIDPP NPs. (b) Dynamic light scattering of PDIDPP NPs in water. (c) Normalized absorbance spectra of PDIDPP in THF and NPs in water. (d) Normalized fluorescence spectra of PDIDPP in THF and NPs in water.

High photothermal conversion efficiency promises excellent therapeutic efficacy. The heating curve of the PDIDPP NPs in distilled water with irradiation or the cooling curve without irradiation was recorded (Fig. 2c). A temperature elevation of 25.2 °C with laser irradiation in the presence of PDIDPP was observed and the photothermal conversion efficiency is calculated as 32.6% (Fig. 2d), which is higher than that of the previously reported (*E*)-3-(4-(dimethylamino)styryl)-5,5-difluoro-2,8-diiodo-1,7,9-trimethyl-10-phenyl-5*H*-di-pyrrolo[1,2-*c*:20,10-*f*][1,3,2] diazaborinin-4-ium-5-uide (28.6%)³⁵ but lower than that of 3,6-bis(5-(4-(9*H*-carbazol-9-yl)phenyl)furan-2-yl)-2,5-bis(2-octyldodecyl)pyrrolo[3,4-*c*]pyrrole-1,4(2*H*,5*H*)-dione (48.2%)²⁵ or NDT (65.6%)²⁷ or PTVT (52.6%).²⁸ The photostability of PDIDPP is very high because no absorbance decay has been observed after laser irradiation (Fig. S4, ESI[†]).

In vitro cellular uptake and MTT assay

The cellular uptake of PDIDPP NPs *in vitro* was investigated by confocal laser scanning microscopy (CLSM). PDIDPP NPs can be efficiently uptaken by U87MG and HCT-116 cells, as indicated by the red channel (Fig. 3). With laser irradiation, strong singlet oxygen generation could be observed due to the strong green fluorescence of DCF (Fig. 3). After incubation for 24 h, the dark or photo toxicity was determined by MTT assay. For the dark group, the cytotoxicity is dependent upon the concentration, suggesting the low dark toxicity of PDIDPP NPs (Fig. 4a and b). On the contrary, the cytotoxicity with irradiation shows

concentration-dependent death and the half maximum inhibitory concentration (IC_{50}) of PDIDPP NPs is 25.8 and 28.3 $\mu\text{g mL}^{-1}$ on U87MG and HCT-116 cells, respectively (Fig. 4a and b). The therapeutic efficacy of PDT or PTT only has been investigated by using a 37 °C water bath to maintain a suitable temperature or adding glutathione (GSH) as the ROS scavenger (Fig. S5 and S6, ESI[†]). The individual therapy is less effective than the synergistic therapy because the IC_{50} is much higher. The results demonstrate that PDIDPP NPs have the potential for PDT/PTT synergistic therapy. Cell apoptosis was further investigated by flow cytometry (Fig. 4c). For the control group, negligible cell death was observed because the apoptosis rate is very low (0.03% for U87MG and 0.02% for HCT-116, respectively). The same phenomenon was found in the group treated with PDIDPP NPs without irradiation (1.26% for U87MG and 0.08% for HCT-116 cells, respectively), indicating the low dark toxicity of these NPs. Significant cell apoptosis induced by a laser further suggests the high phototoxicity of the NPs because the cell apoptosis rate is much higher than those in the control and non-irradiation groups (21.28% for U87MG and 20.80% for HCT-116 cells, respectively).

In vivo photodynamic and photothermal therapy

15 nude mice bearing U87MG tumors were divided into three groups, including saline + light, PDIDPP NPs only, and PDIDPP NPs + light. To investigate the therapeutic efficacy, the tumor volume and body weight were recorded every two days (Fig. 5a and b). The tumor volume of the mice treated with PDIDPP NPs



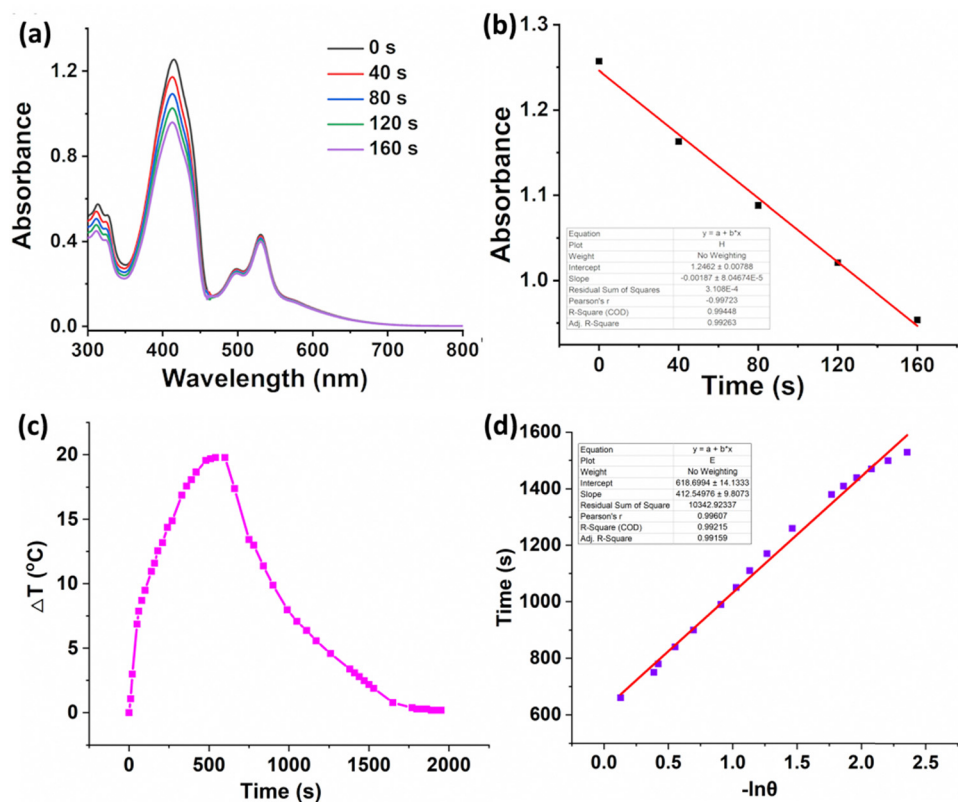


Fig. 2 (a) $^1\text{O}_2$ generation of PDIDPP in dichloromethane using DPBF as a probe (100 mW cm^{-2}). (b) Linear fitting of time versus absorbance. (c) Temperature elevation and decrease curve of PDIDPP NPs with or without irradiation (660 nm , 0.5 W cm^{-2}). (d) Linear fitting of $\ln \theta$ versus time.

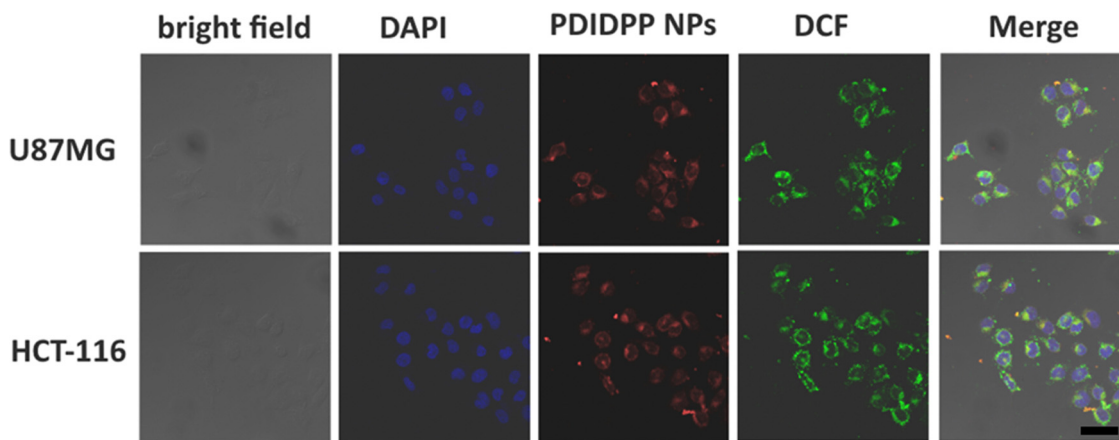


Fig. 3 *In vitro* cellular uptake and ROS generation of PDIDPP NPs in U87MG and HCT-116 cells with DCF as a probe (660 nm , 0.5 W cm^{-2}). Scale bar: $10 \mu\text{m}$.

is similar to that of the control group, indicating the low dark toxicity of TDPP NPs themselves.^{36–39} In comparison, obvious tumor suppression was observed for those treated with PDIDPP NPs with the help of light. Tumors in the PDIDPP NPs + light group disappeared thoroughly. Consistently, the body weight in the three groups all kept increasing, suggesting the low toxicity of the NPs, regardless of light irradiation or not. The mice were then sacrificed and the tumors, heart, liver, spleen, lungs, and

kidneys were collected. According to the hematoxylin and eosin (H&E) stained images of the tumors, the nucleus in the control and PDIDPP NPs only group remained complete (Fig. 5c and d). The results indicated that PDIDPP NPs exerted anti-tumor activity without any toxicity *in vivo*. The H&E stained pictures of the normal tissues are illustrated in Fig. 5e. These cells are all in a good manner, further confirming the excellent biocompatibility of such NPs.^{40–42}



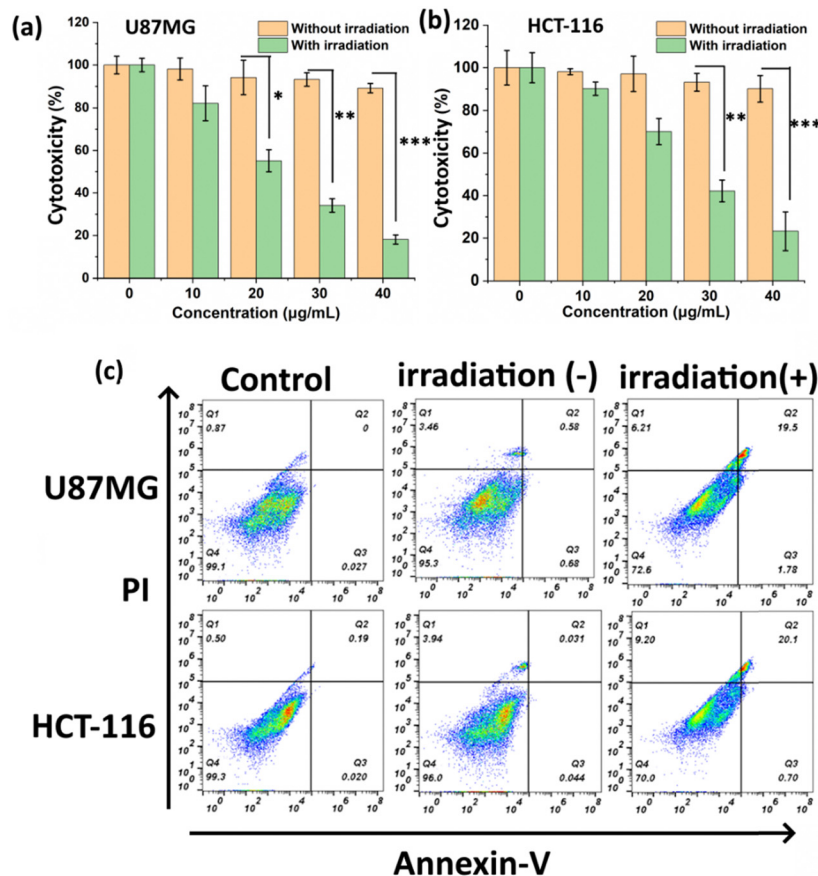


Fig. 4 (a) MTT assay of PIDIDPP NPs on U87MG and (b) HCT-116 cells with or without irradiation (660 nm, 0.5 W cm^{-2} , $**P < 0.01$, $***P < 0.001$). (c) Flow cytometry of PIDIDPP NPs on U87MG and HCT-116 cells at the concentration of $10 \mu\text{g mL}^{-1}$.

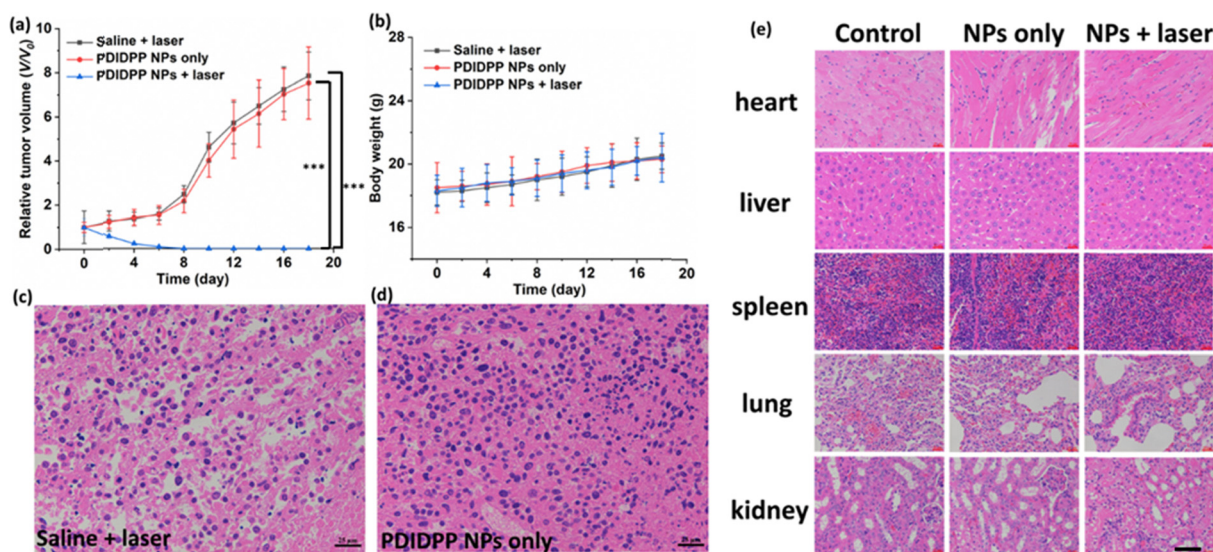


Fig. 5 (a) Relative tumor volume, (b) body weight of nude mice treated with saline, PIDIDPP NPs only and PIDIDPP NPs + light. H&E stained tumor pictures in the (c) control and (d) PIDIDPP NPs only groups. (e) H&E stained pictures of the heart, liver, spleen, lungs and kidneys in the control, PIDIDPP NPs only and PIDIDPP NPs + light groups. Scale bar: $25 \mu\text{m}$.



Conclusions

In summary, a heavy atom free photosensitizer (PDIDPP) was synthesized and prepared by a simple C–H activation reaction. PDIDPP NPs prepared by nanoprecipitation with both singlet oxygen generation ability and photothermal conversion efficiency show excellent phototoxicity against cancer cells (U87MG and HCT-116). With light irradiation, PDIDPP NPs can induce efficient cell apoptosis on U87MG and HCT-116 cells, which has been confirmed by both MTT assay and flow cytometry. Meanwhile, the dark toxicity of PDIDPP NPs is almost negligible. *In vivo* study also confirmed the complete tumor regression of the mice treated with PDIDPP NPs with the assistance of light, compared with those in the control and PDIDPP NPs only groups. Our results suggest that PDIDPP NPs with low dark toxicity, and high phototoxicity have some potential for cancer treatment.

Conflicts of interest

The authors declare no conflict of interest.

Acknowledgements

The authors acknowledge the financial support from Kunshan Hospital Affiliated to Jiangsu University (Grant No. CXTD21-D02), Scientific Research Pre-Technology Development project of Guilin city (No. 20180104-10), and First-class Discipline in Guangxi of Traditional Chinese Pharmacology (Direction of Ethnic Medicine) (2018 No. 12).

References

- R. L. Siegel, K. D. Miller, H. E. Fuchs and A. Jemal, *CA Cancer J. Clin.*, 2021, **71**(1), 7–33.
- N. Shivran, M. Tyagi, S. Mula, P. Gupta, B. Saha, B. S. Patro and S. Chattopadhyay, *Eur. J. Med. Chem.*, 2016, **122**, 352–365.
- M. Laine, N. A. Barbosa, A. Kochel, B. Osiecka, G. Szewczyk, T. Sarna, P. Ziolkowski, R. Wieczorek and A. Filarowski, *Sens. Actuators, B*, 2017, **238**, 548–555.
- A. Carija, N. Puizina-Ivic, D. Vukovic, L. Miric Kovacevic and V. Capkun, *Photodiagn. Photodyn. Ther.*, 2016, **16**, 60–65.
- W. P. Fan, P. Huang and X. Y. Chen, *Chem. Soc. Rev.*, 2016, **45**, 6488–6519.
- Z. Yang, Y. L. Dai, L. Shan, Z. Y. Shen, Z. T. Wang, B. C. Yung, O. Jacobson, Y. Liu, W. Tang, S. Wang, L. Lin, G. Niu, P. Huang and X. Chen, *Nanoscale Horiz.*, 2019, **4**, 426–433.
- J. Yang, X. Q. Gu, W. T. Su, X. Y. Hao, Y. J. Shi, L. Y. Zhao, D. F. Zou, G. W. Yang, Q. Y. Li and J. H. Zou, *Mater. Chem. Front.*, 2018, **2**, 1842–1846.
- J. Yang, Y. Xu, M. Jiang, D. F. Zou, G. W. Yang, L. Shen and J. H. Zou, *J. Inorg. Biochem.*, 2019, **193**, 124–129.
- J. Shen, J. J. Chen, Z. Ke, D. F. Zou, L. G. Sun and J. H. Zou, *Mater. Chem. Front.*, 2019, **3**, 1123.
- J. H. Zou, P. Wang, Y. Wang, G. Y. Liu, Y. W. Zhang, Q. Zhang, J. J. Shao, W. L. Si, W. Huang and X. C. Dong, *Chem. Sci.*, 2019, **10**, 268–276.
- J. H. Zou, L. Xue, N. Yang, Z. Fan, W. J. Wang, W. L. Si, Y. W. Zhang, W. Huang and X. C. Dong, *Mater. Chem. Front.*, 2019, **3**, 2143–2150.
- J. H. Zou, Z. H. Yin, K. K. Ding, Q. Y. Tang, J. W. Li, W. L. Si, J. J. Shao, Q. Zhang, W. Huang and X. C. Dong, *ACS Appl. Mater. Interfaces*, 2017, **9**, 32475–32481.
- I. Turan, D. Yildiz, A. Turksoy, G. Gunaydin and E. Akkaya, *Angew. Chem., Int. Ed.*, 2016, **55**, 2875–2878.
- Y. Cakmak, S. Kolemen, S. Duman, Y. Dede, Y. Dolen, B. Kilic, Z. Kostereli, L. Yildirim, A. Dogan, D. Guc and E. Akkaya, *Angew. Chem., Int. Ed.*, 2011, **50**, 11937–11941.
- D. Xi, M. Xiao, J. Cao, L. Zhao, N. Xu, S. Long, J. Fan, K. Shao, W. Sun, X. Yan and X. Peng, *Adv. Mater.*, 2020, **32**, 1907855.
- J. H. Zou, L. Li, Z. Yang and X. Y. Chen, *Nanophotonics*, 2021, **10**(12), 3229–3245.
- L. Li, J. H. Zou, Y. L. Dai, W. P. Fan, G. Niu, Z. Yang and X. Y. Chen, *Nat. Biomed. Eng.*, 2020, **4**(11), 1102–1116.
- J. H. Zou, L. Li, J. W. Zhu, X. Z. Li, Z. Yang, W. Huang and X. Y. Chen, *Adv. Mater.*, 2021, 2103627.
- W. Sun, R. Thiramanas, L. D. Slep, X. L. Zeng, V. Mailänder and S. Wu, *Chem. – Eur. J.*, 2017, **23**, 10832.
- W. Sun, S. Y. Li, B. Haupler, J. Liu, S. B. Jin, W. Steffen, U. S. Schubert, H. J. Butt, X. J. Liang and S. Wu, *Adv. Mater.*, 2017, **29**, 1603.
- K. Fujita, Y. Y. Tanaka, T. Sho, S. C. Ozeki, S. Abe, T. Hikage, T. Kuchimaru, S. K. Kondoh and T. Ueno, *J. Am. Chem. Soc.*, 2014, **136**, 16902.
- J. C. Li, D. Cui, Y. Jiang, J. Huang, P. Cheng and K. Y. Pu, *Adv. Mater.*, 2019, **31**(46), e1905091.
- J. H. Zou, J. W. Zhu, Z. Yang, L. Li, W. P. Fan, L. C. He, W. Tang, L. M. Deng, J. Mu, Y. Y. Ma, Y. Y. Cheng, W. Huang, X. C. Dong and X. Y. Chen, *Angew. Chem., Int. Ed.*, 2020, **59**, 8833.
- J. C. Li, J. G. Huang, Y. Lyu, J. Huang, Y. Jiang, C. Xie and K. Y. Pu, *J. Am. Chem. Soc.*, 2019, **141**(9), 4073–4079.
- J. Deng, N. Zhong, X. C. Zhang, C. Li, C. Xu and J. Zhao, *J. Mater. Chem. B*, 2020, **8**(47), 10764–10769.
- J. C. Li, D. Cui, J. Huang, S. S. He, Z. Yang, Y. Zhang, Y. Luo and K. Y. Pu, *Angew. Chem., Int. Ed.*, 2019, **58**(36), 12680–12687.
- Y. L. Gu, G. Q. Zhou, Y. J. Zhong, L. T. Tan, Z. H. Zheng, Z. H. Qiu, B. Wei, L. Shen, J. Yang and D. F. Zou, *Mater. Chem. Front.*, 2022, **6**, 8.
- X. J. Zhang, A. L. Zhang, J. F. Feng, J. Yi, L. Peng, J. J. Chen, Z. Ke, J. Yang, Y. S. Dai and D. F. Zou, *Mater. Des.*, 2021, **197**, 109263.
- X. Li, G. Zhang and Y. Tang, *BME Front.*, 2020, 2095460.
- W. Tahir, S. Kura, J. Zhu, X. Cheng, R. Damseh, F. Tadesse, A. Seibel, B. Lee, F. Lesage, S. Sakadžic, D. Boas and L. Tian, *BME Front.*, 2021, 8620932.
- W. Zhang, I. Oraiqat, H. Lei, P. Carson, I. Ei Naqa and X. Wang, *BME Front.*, 2020, 9853609.
- J. Shen, L. Pan, X. Zhang, Z. Zou, B. Wei, Y. Chen, X. Tang and D. Zou, *Front. Bioeng. Biotech.*, 2022, **10**, 781766.
- Z. Li, J. Zou and X. Chen, *Adv. Mater.*, 2023, 2209529.



- 34 Z. Yang, W. P. Fan, J. H. Zou, W. Tang, L. Li, L. C. He, Z. Y. Shen, Z. T. Wang, O. Jacobson, M. A. Aronova, P. F. Rong, J. B. Song, W. Wang and X. Y. Chen, *J. Am. Chem. Soc.*, 2019, **141**(37), 14687–14698.
- 35 D. Zou, A. Zhang, J. Chen, Z. Chen, J. Deng, G. Li, S. Zhang, Z. Feng, J. Feng and J. Yang, *Mater. Chem. Front.*, 2021, **5**, 2694.
- 36 X. Hu, C. Zhu, F. Sun, Z. Chen, J. Zou, X. Chen and Z. Yang, *Adv. Mater.*, 2023, DOI: [10.1002/adma.202304848](https://doi.org/10.1002/adma.202304848).
- 37 J. Cheng, Y. Zhu, Y. Dai, L. Li, M. Zhang, D. Jin, M. Liu, J. Yu, W. Yu, D. Su, J. Zou, X. Chen and Y. Liu, *Angew. Chem., Int. Ed.*, 2023, e202304312.
- 38 J. Zhu, Y. Zhang, Z. Li, X. Bao, Y. Zhou, B. Ma, Y. Xie, P. Yan, Z. Wu, Q. Zhang, J. Zou and X. Chen, *Mater. Horiz.*, 2023, **10**, 3014–3023.
- 39 X. Li, Z. Xiong, X. Xu, Y. Luo, C. Peng, M. Shen and X. Shi, *ACS Appl. Mater. Interfaces*, 2016, **8**(31), 19883–19891.
- 40 X. Li, H. Sun, H. Li, C. Hu, Y. Luo, X. Shi and A. Pich, *Adv. Funct. Mater.*, 2021, **31**, 2100227.
- 41 X. Li, L. Hetjens, N. Wolter, H. Li, X. Shi and A. Pich, *J. Adv. Res.*, 2023, **43**, 87–96.
- 42 Y. Lu, Q. Luo, X. Jia, J. Tam, H. Yang, Y. Shen and X. Li, *J. Pharm. Anal.*, 2023, **13**, 239–254.

